Fluid hydrogen at high density: Pressure ionization

Didier Saumon
Lunar and Planetary Laboratory, University of Arizona, Tucson, Arizona 85721

Gilles Chabrier
Laboratoire de Physique, Ecole Normale Supérieure de Lyon, 69364 Lyon CEDEX 07, France
(Received 18 February 1992)

In an earlier paper [Phys. Rev. A **44**, 5122 (1991)], we presented a Helmholtz-free-energy model for nonideal mixtures of hydrogen atoms and molecules. In the present paper, we extend this model to describe an interacting mixture of H_2, H, H^+, and e^- in chemical equilibrium. This general model describes the phenomena of dissociation and ionization caused by pressure and temperature effects, as encountered in astrophysical situations and high-pressure experiments. The present model is thermodynamically unstable in the pressure-ionization regime and predicts the existence of a plasma phase transition with a critical point at $T_c = 15\,300$ K, $P_c = 0.614$ Mbar, and $\rho_c = 0.35$ g/cm^3. The transition occurs between a weakly ionized phase and a partially ($\approx 50\%$) ionized phase. Molecular dissociation and pressure ionization occur in the same narrow density range; atoms play a minor role in pressure ionization. In the high-density phase, complete pressure ionization is reached gradually. The sensitivity of the coexistence curve and of the critical point to model parameters and assumptions is discussed in detail.

PACS number(s): 52.25.Jm, 64.70.−p, 05.70.−a, 65.50.+m

I. INTRODUCTION

The similarities between hydrogen and alkali metals suggest that pressure-ionized hydrogen would behave like a conducting monovalent "metal" [1] even at zero temperature, and it has often been argued that a first-order phase transition must occur between the two states given the large density difference between the insulating molecular and the conducting metallic states [2–4]. Most of the recent investigations have focused on the zero-temperature transition, where very sophisticated models can be developed in the absence of thermal effects [5–9]. These calculations indicate that the zero-temperature transition occurs between 1 and 4 Mbar. Static compression experiments are beginning to probe this pressure range. Shock compression experiments [10,11] have clearly established the stability of the fluid molecular phase up to 0.8 Mbar. Measurements of the fundamental vibration frequency of the molecule at $T = 77$ K indicate that it is stable at least up to 2 Mbar [12]. A transition associated with a modification of the electronic structure of solid H_2 has been discovered recently [12,13], with a critical point around $T \approx 150$ K and $P \approx 1.7$ Mbar [14,15], but it is generally agreed that the metallic state, which is believed to occur around 2–3 Mbar, has not been observed yet.

Even though the existence of the metal-insulator transition in hydrogen is well established at 0 K (on theoretical grounds), little can be said of it at temperatures of a few thousand degrees and considerable uncertainty remains concerning the form of the phase diagram. The existence of a plasma phase transition (PPT) in the fluid regime between an insulating molecular or atomic phase and a pressure-ionized, metallic fluid phase, and of the associated "second critical point," remains speculative to this day.

In an earlier paper [16] (hereafter, Paper I), we developed a free-energy model for a H-H_2 mixture to describe temperature and pressure dissociation of molecules. In this model the configuration free energy arising from the particle interactions is based on realistic interatomic potentials, and is calculated within the framework of an extended fluid perturbation theory. The influence of the interactions on the internal levels of atoms and molecules is calculated self-consistently with an occupation probability formalism [17]. This free-energy model successfully compares with available shock-wave experiments [11] and Monte Carlo simulations [16,18]. It predicts that pressure dissociation occurs over a narrow density range above $\rho \approx 0.5$ g/cm^3.

In the present paper, we extend this so-called "neutral model" in the pressure and temperature ionization region and present detailed results on pressure ionization and the PPT of hydrogen. In Sec. II we summarize briefly the model developed for the *fully ionized* part of the phase diagram (see Fig. 1 of Paper I). This model has been described in detail elsewhere [19] and is summarized here for completeness. In Secs. III and IV, we present the free-energy model, which describes partial ionization. Section V is devoted to an extended analysis of the PPT predicted by our model. The thermodynamics and the behavior of our model are discussed in Sec. VI.

II. FULLY IONIZED MODEL

At temperatures such that $kT \gtrsim 1$ Ry, or for densities such that the Fermi energy is greater than 1 Ry, hydrogen is fully ionized and constitutes a fluid mixture of protons and electrons subject to Coulomb forces. The model

we developed in this region [19] relies on the so-called two-fluid model, used extensively in liquid-state theory [20]. Within this model, the plasma is equivalent to the superposition of two uncoupled fluids: a jellium electron gas and a fluid of pseudoions interacting through the short-range *screened* potential

$$V^{\text{eff}}(K)=\frac{4\pi(Ze)^2}{K^2\epsilon(K)}\ , \tag{1}$$

where Ze is the ionic charge and $\epsilon(K)$ denotes the electron dielectric function for wave number K. This so-called screened one-component plasma model (SOCP) relies on two assumptions in the treatment of the response of the electron gas, namely the adiabatic (Born-Oppenheimer) approximation, and the linear-response theory (LRT). The validity of the former approximation has been assessed even in the region of weak degeneracy for the electron gas by comparison with nonadiabatic calculations [21]. The second approximation assumes that as long as the ion-electron potential energy e^2/a, where a is the ion sphere radius, is smaller than the electron Fermi energy ε_F, the electron-ion interaction is weak compared with the kinetic contribution of the electrons and can be treated as a perturbation, retaining the linear contribution only. This point will be discussed in detail below. Given these approximations, the characteristic Helmholtz free energy of the SOCP reads

$$\begin{aligned}F_{\text{SOCP}}&=-kT\ln[\text{Tr}e^{-\beta H}]\\&=F_i^{\text{id}}+F_e^{\text{id}}+F_e^{\text{xc}}-kT\ln\int d\mathbf{R}_1\cdots d\mathbf{R}_N e^{-\beta V^{\text{eff}}}\ ,\end{aligned} \tag{2}$$

where the trace of the Hamiltonian H is taken over the states of the coupled electron-ion system and $\beta=1/kT$. The superscript id denotes the noninteracting contribution to the free energy given either by the standard classical equations for the ions or by the Fermi integrals for the electrons. The last two terms on the right-hand side of Eq. (2) denote respectively the nonideal contributions arising from the electron background and from the screened ionic fluid. For the electron exchange and correlation contribution F_e^{xc}, we used a parametrized thermodynamic function [22] based on calculations of the interaction energy of an electron gas at *finite temperature*, using the Singwi-Tosi-Land-Sjölander (STLS) theory [23] to treat the strong-coupling effects between electrons. The known violation of the compressibility sum rule in the STLS scheme is taken into consideration by anticipating similar deviations in the parametrization. The resulting free energy and its temperature and density derivatives reproduce the classical results [24] and the zero-temperature results [25,26] with deviations of less than 0.6%. In the region of intermediate degeneracy ($\Theta=kT/\varepsilon_F\approx 1$), the authors claim a total error of $\sim 5\%$ on F_e^{xc}.

The thermodynamic functions of the screened ionic fluid were calculated within the framework of the hypernetted-chain theory. The electronic dielectric function entering the effective screened potential [Eq. (1)] is the *finite-temperature* Lindhard dielectric function [27], corrected with a temperature-dependent local-field correction [28,21]. The resulting thermodynamic functions reproduce existing Monte Carlo calculations in the limit of the rigid electron background ($r_s=a/a_0=0$, a_0 being the Bohr radius) [24], zero-temperature random-phase approximation [29], and finite-temperature random-phase approximation [30] within less than 1% [19]. In the low-temperature, high-density region of the phase diagram (see Fig. 1 of Paper I), we can expect quantum effects on the ions to become important. In the density domain where pressure ionization occurs, however, the quantum contribution to the thermodynamics is small ($\lesssim 0.3\%$) and it is described by the Wigner-Kirkwood $\hbar^2$ correction [31].

In the high-temperature ($kT>1$ Ry), intermediate-density ($2<r_s<10$) range, the thermodynamic functions of the plasma were interpolated with the so-called two-component-plasma model [32,33], which recovers the Debye-Hückel limit at low density (see Ref. [19] for details).

Finally a term F_0 was added to the plasma free energy to make the fully ionized model compatible with the neutral model. Since we have included the proton spin in the neutral model and we must use the same zero point for the energy scale, which we have chosen as the ground state of the H_2 molecule, we have

$$\frac{\beta F_0}{N_{H^+}}=\ln 2+127\,736.3\beta hc\ , \tag{3}$$

where N_{H^+} is the number of protons and h and c are the Planck constant and the speed of light, respectively.

The main sources of uncertainty in our free-energy model for the fully ionized domain of the phase diagram come essentially from the fit for F_e^{xc} and from the exclusion of nonlinear screening effects in the SOCP model. Recent calculations using the inherently nonlinear density-functional theory (DFT) for the ion-electron interaction show that nonlinear effects in the hydrogen plasma are already significant for $r_s\approx 1$ at $\theta\approx 0.1$ [34]. Other calculations based on the density-response formalism [35] seem to agree with the DFT results for $r_s\lesssim 1$, where no bound states are involved. Comparison between these calculations and our SOCP model for $r_s=1$ show an appreciable difference ($\approx 15\%$) on the excess *interaction* energy for $\Gamma=e^2/akT\approx 1-5$, corresponding to $\Theta\approx 0.1-0.5$. This discrepancy drops to $\approx 2-5\%$ when comparing the excess *internal* and free energies, and then to $\approx 2\%$ on the *total* free energy. At higher temperatures the electron cloud becomes more and more uniform, and the LRT becomes accurate [for $\Gamma=1$ and $r_s=1$, the ion-ion pair-correlation function and effective potentials derived from Eq. (1) are found to be indistinguishable from the DFT results [36]]. For lower temperatures, the kinetic energy of the electrons is larger than the interaction energy and we can expect nonlinear effects to be less significant. In any event, nonlinear calculations for the ion-electron interaction have been computed over a very narrow (Γ, r_s) range, and we must rely on the simpler

SOCP model for the extensive computations necessary for the construction of a phase diagram.

Given the shortcoming of the LRT and the error claimed on F_e^{xc} we estimate the resulting maximum error from both of the sources to be $\approx 5\%$ on the *total* free energy of the plasma, a value reached when $\Gamma \approx 1-5$ and $r_s = 1$. On the other hand, the fully ionized free-energy model represents only one contribution to our general model, which does include an explicit treatment of bound states and consequently nonlinear effects in the region of partial ionization. As will be shown below, our model predicts bound states for $r_s \geq 1$, which puts a low-density limit on the fully ionized model.

III. PARTIAL IONIZATION

In Paper I and in the previous section, we have presented the two models used for the two extreme limits of the phase diagram: the fully ionized regime at high temperatures ($\log_{10} T \gtrsim 5.6$) or at high densities ($\log_{10}\rho \gtrsim 0.5$) [37] and the domain where only atoms and molecules coexist ($\log_{10} T \lesssim 4.0$, $\log_{10}\rho \lesssim -0.5$). The remaining area between these two regions is the domain of partially ionized matter. At low densities, the gas is nearly ideal and ionization is a temperature effect described by the Saha equations, centered on a roughly constant temperature ($\log_{10} T \approx 4.3$). At a density of $\log_{10}\rho \approx 0$ and at temperatures below the regime of temperature ionization, pressure effects are responsible for ionization.

We now combine these two limiting models in a *single* model for the Helmholtz free energy of a system of H_2, H, H^+, and e^-, intended to describe dissociation and ionization caused by temperature and pressure effects. In reality, H_2^+, H_3^+, and H^- ions are also present when ionization is incomplete. The computations of Hummer and Mihalas [17,38] reveal that the concentration of H^- peaks at $\log_{10} T = 4.05$ and $\log_{10}\rho = -3.00$ with a value of 1.2×10^{-4}, while the corresponding values for H_2^+ are $\log_{10} T = 4.20$, $\log_{10}\rho = -2.80$, and 6.2×10^{-4}, respectively. Estimates based on our model indicate that the concentration of H_3^+ remains everywhere below 2×10^{-3}. These concentrations are small and the contributions of these ions can be neglected in an equation of state (EOS) calculation.

A. Coupling between the two models

1. Stark ionization

An important form of coupling between charged and neutral particles involves the dissolution of high-lying states into the continuum of free electrons through Stark ionization caused by the fluctuating electric microfield of the plasma. The dissolution of states directly affects the internal partition function (IPF) of atoms and molecules. In our model, the effect of interactions on the IPF is described with an occupation probability formalism [16,17]. The occupation probability ω_α of state α due to Stark ionization is given by [17]

$$\omega_\alpha = \int_0^{E_\alpha^{\rm crit}} P(E)dE \ . \tag{4}$$

Here, $P(E)$ is the statistical distribution of the field of magnitude E and $E_\alpha^{\rm crit}$ is the minimum electric field necessary to induce Stark ionization of level α. Hummer and Mihalas [17] used the infinite-temperature Holtsmark microfield distribution, which neglects the correlations among the charged particles entirely ($\Gamma = 0$). While this is an acceptable approximation in the low-density, high-temperature regime of the ionized EOS ($\Gamma \ll 1$), it is inadequate for a description of pressure ionization, where $10 < \Gamma < 40$ typically. It is possible to go beyond the Holtsmark approximation (see, e.g., Ref. [39]) but the complexity of these calculations makes it virtually impossible to include them in our model. For values of the critical field typical of the ground state of atomic hydrogen, we found that the occupation probability given by Eq. (4) is quite sensitive to the Γ dependence of the microfield distribution and could be underestimated by up to an order of magnitude.

Inclusion of Stark ionization in our model, with the Holtsmark distribution for the microfield, causes the equilibrium state to jump directly from *zero* ionization to *full* ionization. This is caused by the very rapid rise of the importance of the microfield term with density, a coupling so strong as to prevent charged and neutral particles from coexisting! This behavior persists to temperatures up to and above $\log_{10} T = 5.5$, at which point it is generally agreed that ionization proceeds smoothly with increasing density.

Clearly, treating Stark ionization with the Holtsmark distribution is inappropriate in the regime of pressure ionization. In Sec. V B 1, we estimate quantitatively *ex post facto* the importance of Stark ionization in the regime of pressure ionization and find that it is small.

2. Polarization potential

At high density, the nonideal interactions between atoms and plasma could be well represented by approximating atoms by polarizable hard spheres imbedded in a plasma. A conceptually similar idea is to use pseudopotentials to describe the charged-neutral interactions. We adopt a simple approach that describes the interaction between charged and neutral particles with a polarization potential [40,41]:

$$V_i^{\rm pol}(r,R_i) = -\frac{e^2\alpha_i}{2}\left[\frac{1+r\kappa}{r^2+R_i^2}\right]^2 e^{-2\kappa r} \ . \tag{5}$$

Here, R_i and α_i are the hard-core radius of the polarization potential and the polarizability of species i, respectively, and κ is the inverse screening length of the plasma given by [19]

$$\kappa^2 = \frac{3\pi e^2}{kT}\frac{N_e}{V}\Theta^{3/2} I_{-1/2}(\beta\mu_e) \ , \tag{6}$$

where N_e is the number of electrons, V is the volume, and $I_{-1/2}(\beta\mu_e)$ is the Fermi integral for a free-electron gas with chemical potential μ_e. The potential (5) clearly in-

terpolates between a hard-sphere potential at small distances, which represents the Pauli exclusion principle, and the $1/r^3$ characteristic behavior of polarization effects at large distances, weighted by the plasma screening function. The screening length $1/\kappa$ is the one entering the screened Coulomb potential when no local-field correction is included in the electron dielectric function. It ensures consistency of the charge-charge screened potential in the fully and partially ionized regions. This expression clearly reduces to the Debye-Hückel and Thomas-Fermi screening lengths when ($\Gamma \ll 1$ and $\Theta \gg 1$) and ($r_s \ll 1$ and $\Theta \ll 1$), respectively. Given the arbitrariness of the choice of a characteristic screening length for the whole plasma in the polarization potential [Eq. (5)], we examine the sensitivity of our results on this quantity in Sec. V.

The polarization of atoms and molecules introduces an additional term in the free energy [41]:

$$F_{\rm pol}=\frac{2kT}{V}\sum_{i=1}^{2} N_i(N_e B_{i,e^-}+N_{\rm H^+}B_{i,\rm H^+}) , \tag{7}$$

where the sum is over neutral species only, N_i is the number of particles of species i, and B_{i,e^-} and $B_{i,\rm H^+}$ are the second virial coefficients of the polarization potential between neutral species i and electrons or protons, respectively. Since electrons and protons are point charges with charge $|Z|=1$, the virial coefficients are given by

$$B_{i,e^-}=B_{i,\rm H^+}=2\pi\int_{R_i}^{\infty}(1-e^{-\beta V_i^{\rm pol}(r,R_i)})r^2dr\equiv B_i . \tag{8}$$

Using Eq. (8) and the electroneutrality condition, we rewrite the polarization free energy as

$$F_{\rm pol}=4kT\frac{N_e}{V}\sum_{i=1}^{2} N_i B_i . \tag{9}$$

To proceed, we must specify the R_i. Following Ebeling *et al.* [41], we elected to use the diameters entering the configuration energy, given in our case by the Weeks-Chandler-Andersen criterion (see Sec. III B 2 and Fig. 6 of Paper I). There is no physical reason for these diameters to be related, however, and the effect of this choice on our results is examined in Sec. V.

The hard cores in the charged-neutral interactions exclude charged particles from the volume occupied by the atoms and molecules, as defined by their hard-sphere diameters. The free energy of a mixture of four types of hard spheres, two of which having zero diameter (i.e., electrons and protons) is [42]

$$\beta F_{\rm HS}(N_1,N_2,N_3,N_4,\sigma_1,\sigma_2,\sigma_3=0,\sigma_4=0)$$
$$=\beta F_{\rm HS}(N_1,N_2,\sigma_1,\sigma_2)-(N_3+N_4)\ln(1-\eta) , \tag{10}$$

where $\eta=(\pi/6)\sum_i N_i\sigma_i^3/V$ is the hard-sphere packing fraction. The last term on the right-hand side of Eq. (10) can be combined with the ideal energy of a Maxwell-Boltzmann gas [first term in Eq. (24) of Paper I] as a volume renormalization factor $(1-\eta)$. Thus charged-neutral coupling by a polarization potential introduces an additional term into the free energy and excludes the charged particles from penetrating the atoms and molecules by reducing the volume available to the plasma in the *kinetic* terms only.

In summary, the general form of the adopted free-energy model for the four-component mixture of H_2, H, H^+, and e^- reads as follows:

$$F(V,T,N_{\rm H_2},N_{\rm H},N_{\rm H^+},N_e)=F^{\rm id}(V,T,N_{\rm H_2},N_{\rm H})+F^{\rm id}((1-\eta)V,T,N_{\rm H^+},N_e)$$
$$+F_N^{\rm ex}(V,T,N_{\rm H_2},N_{\rm H})+F_I^{\rm ex}(V,T,N_{\rm H^+},N_e)+F_{\rm pol}(V,T,N_{\rm H_2},N_{\rm H},N_{\rm H^+},N_e) , \tag{11}$$

where the superscript id indicates the ideal (kinetic) contribution and $F_N^{\rm ex}$ and $F_I^{\rm ex}$ represent the nonideal contributions from the neutral model and the fully ionized model, given respectively by Eq. (24) of Paper I and by Eq. (2).

B. Chemical equilibrium

We now compute the chemical equilibrium of the four-component mixture of H_2, H, H^+, and e^-. As mentioned in Sec. VI of Paper I, it is more appropriate to minimize the *specific* free energy per proton $\tilde{F}$ with respect to number concentrations $x_i=N_i/N$. The use of the relations

$$\sum_{i=1}^{4} x_i=1, \quad x_{\rm H^+}=x_e \tag{12}$$

leaves only two independent concentrations, which we choose to be x_1 and x_2 (subscripts 1, 2, 3, and 4 refer to H, H_2, H^+, and e^-, respectively). The specific free energy thus depends on four variables $\tilde{F}=\tilde{F}(x_1,x_2,\rho,T)$, where ρ is the *mass* density. The condition for chemical equilibrium can thus be written as

$$\left.\frac{\partial\tilde{F}}{\partial x_1}\right|_{x_2,\rho,T}=\left.\frac{\partial\tilde{F}}{\partial x_2}\right|_{x_1,\rho,T}=0 , \tag{13}$$

which is a two-dimensional minimization of $\tilde{F}$. The minimization algorithm uses Powell's method [43]. Convergence is achieved when the change in the free energy $\tilde{F}$ from one iteration to the next is less than one part in 10^9. The corresponding accuracy in the concentrations is $\Delta x_i\approx 10^{-7}$ for the dominant species.

IV. MODIFICATION OF THE INTERATOMIC POTENTIALS

When we apply the free-energy model [Eq. (11)] with the polarization potential coupling [Eq. (9)] to the com-

putation of pressure ionization, it is found to resist full ionization, predicting small concentrations (a few percent) of neutral particles at very high density, where the fluid must be fully ionized. This is an indication that our model still provides an incomplete description of very dense hydrogen. This is not too surprising since this problem occurs in the high-density regime, where the chemical picture can only provide a caricature of the actual physics of the fluid. While the nature of the coupling between the neutral and fully ionized models certainly affects the degree of ionization, it is wrong to dismiss our choice (polarization potential) on the grounds that we do not reach full ionization with increasing density. The source of the problem lies elsewhere, as shown below. We found in fact that at high density, the free energy of $H+H_2$ is still *lower* than the free energy of the fully ionized plasma, indicating that the minimum of the free energy (i.e., the chemical equilibrium) lies somewhere in between, implying partial ionization. It is then impossible to reach full ionization by simply modifying the nature of the coupling. The problem arises from the uncertainties in the interatomic potentials and from a limited knowledge of the density dependence of the internal partition function. These sources of inaccuracy increase with density.

In the framework of the chemical picture, it can be argued that the rather low free energy of the neutral model is caused by interatomic potentials that are too soft at short range. Since the form of these potentials in the inner-core region ($r \lesssim 1.5$ Å) is unknown, we have introduced an *ad hoc* modification of the interatomic potentials $\phi_{H_2\text{-}H_2}$, $\phi_{H\text{-}H_2}$, and $\phi_{H\text{-}H}$ in this region. We choose to introduce hard-sphere cores into all three potentials, which are now defined by

$$\phi_{ij}(r)=\begin{cases}\infty, & r\le\sigma_{ij}^0\\ \phi_{ij}(r) & \text{otherwise},\end{cases} \tag{14}$$

where $i,j=1,2,\sigma_{ij}^0$ is the fixed *ad hoc* hard-core diameter,

TABLE I. Points along the deuterium Hugoniot curves of Fig. 1 (dotted lines), computed from our model after hard repulsive cores were added to the interaction potentials. See text. The last column gives the concentration of D atoms $x_D=N_D/(N_D+N_{D_2})$.

T (K)	V (cm^3/mol)	P (GPa)	x_D
20.23	23.600	5.65×10^{-4}	0
555	10.890	2.87	0
978	9.870	4.75	0
1674	8.856	7.83	1.2×10^{-6}
2881	7.836	13.2	8.3×10^{-4}
4280	7.100	19.8	0.014
4781	6.895	22.2	0.025
6500	6.393	30.7	0.081
7500	6.218	35.4	0.120
Double shock, reflected from 7.10 cm^3/mol			
5000	5.386	39.4	0.031
6600	4.222	77.3	0.084

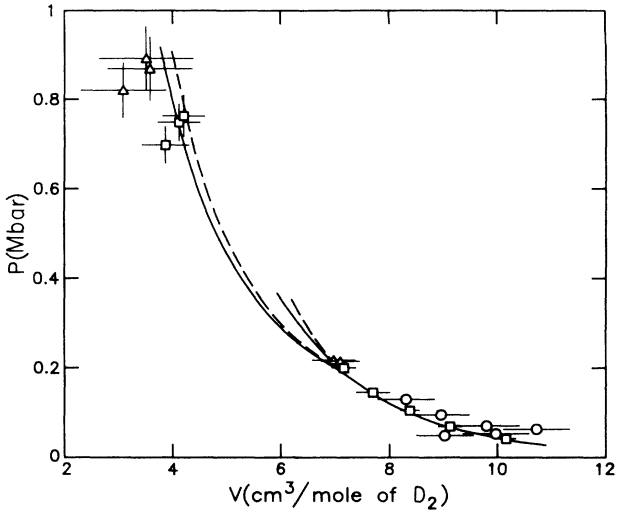

FIG. 1. Single- and double-shock Hugoniot curves of D_2. The experimental data is drawn from Nellis *et al.* [11] (□), Dick and Kerley [71] (○), and Van Thiel *et al.* [10] (△). The solid line shows the theoretical Hugoniot curve which corresponds to Table IV of Paper I. The dashed curve uses the same model but with hard cores introduced into the potentials [Eq. (14)].

and $\phi_{ij}(r)$ is the potential between particles of type i and j, as described in Sec. III A of Paper I. These hard cores represent a modification of the *potentials* themselves, and should not be confounded with the temperature- and density-dependent hard-sphere reference system used to compute the configuration free energy. We have *arbitrarily* fixed the cores of the potentials to be $\sigma_H^0=2.0$ a.u., $\sigma_{H_2}^0=2.7$ a.u., and $\sigma_{H\text{-}H_2}^0=(\sigma_H^0+\sigma_{H_2}^0)/2$. The choice of diameters relies on the intuitive idea that for the H atom the atomic electron becomes unbound and hydrogen atoms lose their identities at distances less than 2 a.u. We assess the effect that these hard cores have on the H_2-H EOS by verifying how they affect the comparison with the experimental results presented in Paper I. The 300-K pressure isotherm of Fig. 3 of Paper I is completely unaffected, for at this temperature the kinetic energy of the molecules is too low to probe the potential at small enough distances to feel the hard core. On the other hand, the presence of the hard cores is felt at the high temperatures reached in double-shock compression experiments. The resulting deuterium Hugoniot curve is shown by the dashed line on Fig. 1 and in Table I. As expected, the theoretical Hugoniot curve is stiffer than before, but it is still in excellent agreement with the experimental measurements, considering the large error bars on the latter.

Clearly the modification of the inner part of the potential has only a minor effect on the comparison of our EOS with experimental results and has the great advantage of producing full ionization at a reasonable density of $r_s\approx1$.

V. PLASMA PHASE TRANSITION

A. Characteristic of the plasma phase transition

Figure 2 shows the behavior of our free-energy model for one isotherm. Each point along the curve is in the

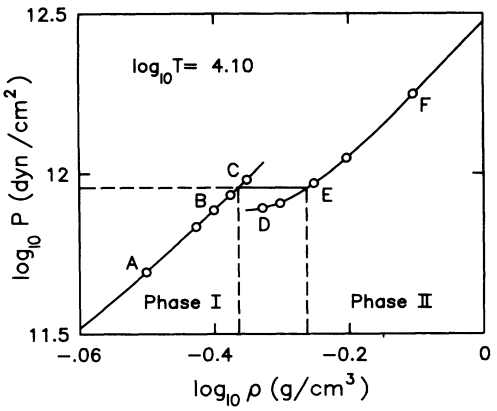

FIG. 2. An isotherm in the region of the PPT ($\log_{10}T=4.10$). Open circles indicate points where the chemical equilibrium was solved numerically. The transition pressure, the metastable region, and the density discontinuity are indicated. The equilibrium concentration of charged particles ($x_{H^+}+x_e=2x_{H^+}$) along the isotherm is *A*, 0.0072; *B*, 0.015; *C*, 0.023; *D*, 0.373; *E*, 0.517; *F*, 0.625.

state of chemical equilibrium, which corresponds to the unique minimum of the free energy [Eq. (11)], obtained by numerically solving Eq. (13). It reveals a discontinuous behavior of the thermodynamic variables, accompanied by a domain of mechanical instability ($\partial P/\partial\rho<0$), which results from a sudden shift of the chemical equilibrium toward a high degree of ionization. We emphasize that this phase change occurs strictly as a result of the minimization of our free-energy model. It does *not* arise from any additional assumption. These are strong indications of the presence of a first-order phase transition.

We have accordingly studied the phase equilibrium in the regime of pressure ionization systematically [44]. The conditions for equilibrium between phases I and II (which we identify as the lower-density insulating phase and the higher-density metallic phase, respectively) are [31]

$$T^{\mathrm{I}}=T^{\mathrm{II}},\quad P^{\mathrm{I}}=P^{\mathrm{II}},\quad \mu_i^{\mathrm{I}}=\mu_i^{\mathrm{II}},\quad i=1,\ldots,4\ , \tag{15}$$

where μ_i^{I} and μ_i^{II} are the chemical potentials of species i in phases I and II, respectively. In the most general case, the chemical potential μ_i depends on six variables

$$\mu_i=\mu_i(x_1,x_2,x_3,x_4,P,T)\ , \tag{16}$$

where $x_i=N_i/N$ is the concentration of species i. The fact that our mixture is in chemical equilibrium imposes four constraints [$\mu_{H_2}=2\mu_H$, $\mu_H=\mu_{H^+}+\mu_e$ and Eq. (12)] on the six independent variables, reducing Eq. (16) to

$$\mu_i=\mu_i(P,T)\ .$$

In other words, at chemical equilibrium, the system is completely specified by P and T. Imposing

$$\mu_H^{\mathrm{I}}(P,T)=\mu_H^{\mathrm{II}}(P,T) \tag{17}$$

at fixed T uniquely determines the transition pressure P for that temperature.

The characteristics of the coexistence curve are given in Table II. The parameters of the critical point are $T_c=15\,300$ K, $P_c=0.614$ Mbar, $\rho_c=0.347$ g/cm^3. The slope of the coexistence curve dP/dT is negative, which is consistent with the positive entropy discontinuity $\Delta S=S^{\mathrm{II}}-S^{\mathrm{I}}$, a likely consequence of the increasing contribution of thermal effects at higher temperature. Our results are compared to other theoretical estimates and to experimental data in Fig. 3.

For comparison, we have also computed a coexistence curve between the neutral and the fully ionized models, where *no mixing* of plasma and atoms or molecules is allowed. We imposed $x_{H^+}=0$ in phase I and $x_{H^+}=1$ in phase II, using $\mu_H^{\mathrm{I}}=\mu_H^{\mathrm{II}}$ to find the phase equilibrium. We refer to this calculation as the "forced" phase transition. This approach is rather artificial since it will produce a phase transition between *any* two models, and it cannot predict a critical point. We find that it overestimates the PPT pressure of our unified model by a factor of 2–3, as shown in Table III and by the dashed line in Fig. 3.

The range of theoretically predicted PPT pressures shown in Fig. 3 spans a full order of magnitude. Most of

TABLE II. Characteristics of the plasma phase transition. For each temperature, we give the transition pressure as well as the density and the ionization fraction for each phase. The change in entropy is $\Delta S=S^{\mathrm{II}}-S^{\mathrm{I}}$. The small differences from Table I of Ref. [44] originate in the correction of an error in the former calculation.

$\log_{10}T$ (K)	P (Mbar)	ρ^{I} (g/cm^3)	ρ^{II} (g/cm^3)	$2x_{H^+}^{\mathrm{I}}$	$2x_{H^+}^{\mathrm{II}}$	ΔS (k_B/proton)
3.70	2.14	0.75	0.92	1.4×10^{-3}	0.48	0.615
3.78	1.95	0.70	0.88	2.1×10^{-3}	0.50	0.590
3.86	1.62	0.64	0.80	3.0×10^{-3}	0.50	0.544
3.94	1.39	0.58	0.74	5.1×10^{-3}	0.51	0.508
4.02	1.13	0.51	0.65	8.8×10^{-3}	0.52	0.464
4.10	0.895	0.43	0.55	0.020	0.50	0.421
4.18	0.631	0.35	0.38	0.17	0.33	0.142
4.185	0.614	0.35		0.18		0

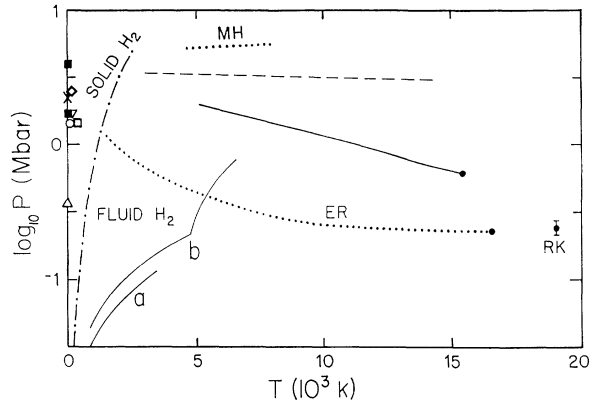

FIG. 3. *P-T* phase diagram for hydrogen in the regime of pressure ionization. Heavy solid line, the PPT and the critical point from the calculations reported in this work (Table II). The dashed line represents the "forced" phase transition given in Table III. Other theoretical estimates for the PPT are labeled MH (Ref. [45]), RK (Ref. [46]), and ER (Ref. [3]). The zero-temperature calculations of Ref.[5] (X) and Ref. [8] (■) for the phase transition are indicated. Dash-dotted curve, theoretical melting curve of H_2 from Ref. [55]. The curves labeled *a* and *b* are experimental single- and double-shock Hugoniot curves H_2 and D_2, respectively [55]. Open symbols indicate the highest pressures reached in static compression experiments: □, Ref. [72]; ○, Ref. [12]; △, Ref. [73]; ◇, Ref. [60]. The critical point of the 150-Mbar transition [14] is shown by an inverted triangle (▽).

this apparent disagreement can be understood in the light of the somewhat crude approximations used in previous efforts.

Marley and Hubbard [45] (MH in Fig. 3) also computed a *forced* phase transition between a neutral and a fully ionized model. Compared to other efforts, their two models are closest to our own in level of accuracy and detail. We attribute most of the difference between the two forced phase transitions to the cruder treatment of the internal levels of the molecules in the MH calculations. From the comparison of the two forced transitions with the PPT obtained by allowing mixing of neutral particles and plasma, it is clear that calculations that forbid mixing of charged and neutral particles overestimate the transition pressure.

The other calculations presented in Fig. 3 allow mixing of plasma and neutral particles and thus "naturally" predict a PPT. The model of Robnik and Kundt (RK) [46] describes a mixture of H, H^+, and e^-. Interactions between neutral and charged particles are neglected, as are the excited states of the atoms. Coulombic terms are computed for a zero-temperature plasma. The H-H interactions are evaluated for both the hard sphere and the Lennard-Jones potentials; their results are insensitive to the form of the interaction. Their critical point lies at $T_c = 19\,000$ K and $P_c = 0.24$ Mbar, shown by the point labeled RK on Fig. 3.

Ebeling and Richert published two calculations for the PPT. Their two models differ in detail but are very similar in spirit and give essentially the same critical point. In Ref. [3], atoms and molecules are present and interact through hard-sphere potentials with a van der Waals correction. Molecules are approximated as two atoms in the hard-sphere free energy. Internal states are not included in the treatment, and there is no coupling between charged and neutral particles. The atomic hard-sphere diameter is *fixed* by calibrating the EOS with laboratory data at the first critical point of hydrogen (liquid-vapor transition, $T_c = 33$ K, $P_c = 13$ bars). They find the second critical point at $T_c = 16\,500$ K, $P_c = 0.228$ Mbar, $\rho_c = 0.13$ g/cm^3. The corresponding coexistence curve is shown as the dotted line in Fig. 3. The approximations for the molecules and for the configuration term of the neutral species (see in particular Sec. VIII A of Paper I), and the absence of internal levels and of coupling between charged and neutral species, are all very crude approximations. Thus it is not surprising that their approximate coexistence curve crosses the experimental double-shock Hugoniot curve for deuterium, where it is generally agreed that there is no evidence for a PPT.

In a second paper, molecules are excluded from the model [4]. Bound states are introduced in the form of the Planck-Larkin partition function, which is incompatible with the chemical picture (see Paper I and Ref. [55] therein). Coupling between neutral and charged species is provided in a fashion similar to that described in Sec. III A 2. However, they renormalize the volume of the electron gas as if it were described by a Maxwell-Boltzmann distribution. This is entirely inappropriate since the electrons are degenerate in the regime of the PPT ($\Theta < 1$). They find a second critical point at $T_c = 16\,500$ K, $P_c = 0.225$ Mbar, surprisingly close to their previous determination.

In all three calculations, the critical pressure P_c is significantly lower than predicted by our model. We attribute this systematic difference to the common use of excessively repulsive hard-sphere or Lennard-Jones potentials between the neutral particles. As discussed in Paper I, these potentials are completely inappropriate in the density range where pressure ionization occurs. Their unrealistically stiff repulsion leads to a very sharp increase in the free energy and the pressure of phase I when the density approaches the value of close packing of hard spheres, and then to an underestimation of the transition pressure.

Recently Yan, Tsai, and Ichimaru [47] (hereafter YTI) also claimed evidence for a PPT at higher temperature.

TABLE III. Characteristics of the forced transition between neutral and fully ionized models. The ionization fraction is 0 in phase I and 1 in phase II, by construction.

$\log_{10}T$ (K)	P (Mbar)	ρ^{I} (g/cm^3)	ρ^{II} (g/cm^3)	ΔS (k_B/proton)
3.60	3.40	0.90	1.20	0.168
3.78	3.34	0.85	1.15	0.086
3.90	3.15	0.80	1.09	0.058
4.00	3.19	0.77	1.05	0.043
4.11	3.09	0.72	0.99	0.040

However we find some of the arguments developed in their conclusion unconvincing. YTI assess the onset of a PPT on the fact that the compressibility derived from their model diverges along a line denoted *AB* (see Figs. 7 and 8 of YTI). Moreover they could not obtain solutions below a line denoted *EF* and associated this behavior with an eventual phase boundary. Line *EF* lies in a low-density range where ionization is mostly temperature induced and described by Saha-like equations. We believe that the divergence of the compressibility in their model is probably due to the inadequacy of the theory to handle bound states. The OCP and the SOCP models will show similar behavior at low enough densities.

Figures (5i) and (5j) of Ref. [46] and Fig. 4 of Ref. [4] indicate that for $T \approx T_c$, full ionization is reached very abruptly as the density is increased. This is not supported by our calculation. Figure 4 shows the concentrations x_{H_2} and $x_{H^+} + x_e = 2x_{H^+}$ for a few isotherms below and above the critical temperature. The degree of ionization increases *very gradually* in phase II for most isotherms. However, in our model, the ionization fraction reaches unity almost discontinuously in a narrow density range ($\rho \approx 2.5 \rightarrow 3.2$ g/cm^3) for all isotherms below $\log_{10} T = 4.66$, with the size of the discontinuity decreasing steadily as the temperature increases. This behavior is not physical and constitutes a flaw in our model and the curves shown in Fig. 4 have been smoothed for $\rho > 2.5$ g/cm^3 for clarity. It is caused by our introduction of hard cores into the interatomic potentials (Sec. IV) and mimics the rapid ionization found in Refs. [46] and [4]. It shows that such an abrupt ionization is probably not physical but rather the consequence of the hard-sphere potentials in the neutral particles interactions.

Based on the characteristics of the PPT as given in Table II and Figs. 3 and 4, we draw the following conclusions.

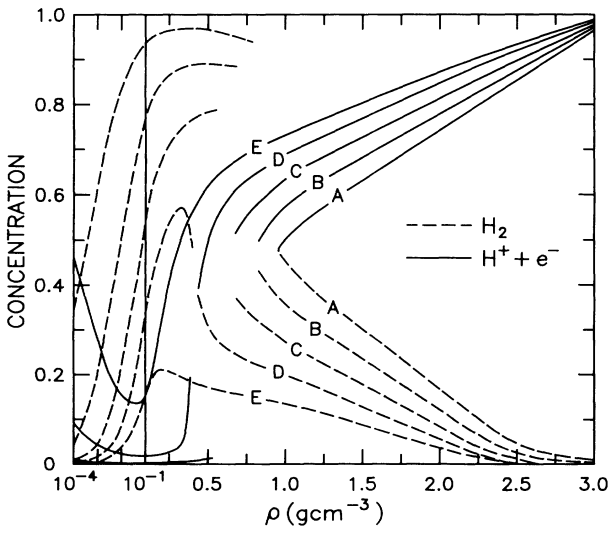

FIG. 4. Concentrations of H_2 and of charged particles ($H^+ + e^-$) near the PPT. Isotherms are labeled according to $\log_{10} T$: *A*, 3.70; *B*, 3.86; *C*, 4.02; *D*, 4.18; *E*, 4.34. The left panel shows the low-density behavior on a log-density scale.

(i) The system undergoes a transition between a *primarily neutral phase* ($2x_{H^+} \lesssim 2\%$) and a *partially ionized phase* ($2x_{H^+} \approx 0.5$). Although the degree of ionization depends on the "free parameters" of the model (hard-core radii in the charged-neutral interaction polarization potential, radii of the hard cores introduced into the atomic interaction potentials), this qualitative feature remains unaffected.

(ii) The PPT persists even in the case where *no coupling* is present between the neutral and the fully ionized models (see V B 1 below). This indicates that the source of the PPT does not lie in the interaction between neutral and charged particles but rather in the very nature of the plasma and the insulating phases.

(iii) The degree of ionization increases drastically and discontinuously at the transition pressure, corresponding to an insulator-metal transition. The most striking feature of this model is that *molecular dissociation and pressure ionization occur almost at the same density* for any temperature. Pressure ionization *does not* occur by first dissociating all molecules into atomic hydrogen as suggested in former calculations [48], but rather directly from the dense molecular fluid. Atomic hydrogen plays a minor role in pressure ionization.

(iv) In phase II, the system reaches complete ionization gradually. The sharp rise in the ionization fraction discussed above (not shown in Fig. 4) does not invalidate this conclusion. Instead, this actually points out the qualitative difference found when treating pressure ionization with more realistic, albeit flawed, potentials as opposed to pure hard-sphere potentials. Even though our model for the neutral species is questionable above the coexistence curve (up to the density where full ionization is reached, $\rho \approx 3$ g/cm^3), our calculations indicate that full ionization may occur much more gradually than suggested by previous studies using hard-sphere potentials.

(v) Molecules are the dominant neutral species at high density. Since their configuration energy, derived from a realistic experimental potential, reproduces both Monte Carlo results [18] and the shock compression data [16], we believe that this effect is real, at least in the low-density phase (phase I). As can be deduced from Fig. 4, the concentration of atomic hydrogen is small near and above the PPT ($x_H \leq 0.1$). This lends credibility to our results since it is clear that in reality (e.g., in the physical picture) it is not possible to distinguish between densely packed hydrogen "atoms" and a strongly correlated ion-electron plasma.

The location of the PPT in density can be compared with the prediction of the simple Herzfeld theory of metallization [49]. This phenomenological theory gives valuable estimates of the metallization densities of a host of elements and diatomic molecules [50]. For atomic and molecular hydrogen it gives metallization densities of 0.600 g/cm^3 and 0.994 g/cm^3, respectively. The Herzfeld critical densities and our PPT are in close agreement.

B. Uncertainties in the plasma phase transition

In this section, we first discuss a limited set of calculations of the PPT using variations on our free-energy mod-

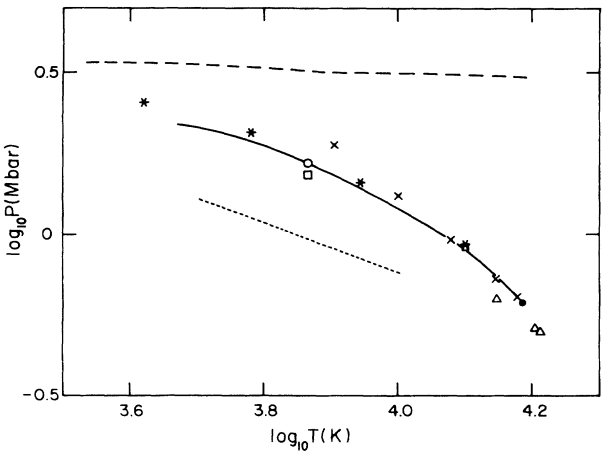

FIG. 5. The effects of various assumptions in the free-energy model upon the plasma phase transition. The solid and dashed curves are coexistence curves for the PPT and for the forced phase transition, respectively, as shown in Fig. 3. The forced phase transition assumes no *mixing* between the neutral and fully ionized models. Hard repulsive cores are included in the interatomic potentials. The crosses (×) indicate the PPT obtained in a calculation where $F_{\rm pol}$ [Eq. (9)] was overestimated by about a factor of 5. The dotted line shows the coexistence curve obtained when using the polarization radius of Ref. [51] in $F_{\rm pol}$. Removing the hard cores leads to the transition pressures shown by the squares (□). When softened interaction potentials are used, the PPT occurs at higher pressures, as shown by the asterisks (*). When no coupling is allowed and hard cores are removed from the interatomic potentials, the transition is shown by the triangles (△). The open circle indicates the effect of softening the lowest vibrational frequency of the H_2 molecule by 4%. See text for details.

el and then estimate the importance of some physical effects that are not included in the model. Figure 5 summarizes the various PPT results. The solid curve is the same PPT as presented in Fig. 3.

1. *Influence of coupling*

The first variation on our final model is indicated by the triangles in Fig. 5. For these calculations, the PPT is computed *without any coupling* between the two models and *without* the hard cores that were introduced into the interatomic potentials. In this model, plasma and neutral particles are allowed to mix but the two fluids do not interact. This corresponds to the free-energy model of Eq. (11) with $\eta=0$ and $F_{\rm pol}=0$. The highest temperature point shown for this calculation ($\log_{10}T_c=4.215$) indicates the corresponding critical point. The second variation is provided using a different expression for the screening length of the plasma [Eq. (6)] so that the polarization free energy $F_{\rm pol}$ [Eq. (9)] is increased by about a factor of 5. This results in the coexistence curve indicated by crosses, with the critical point at $\log_{10}T_c=4.175$.

The third variation is to use the polarization radius for atomic H determined by Redmer, Röpke, and Zimmermann [51], $R_{\rm H}=1.4565$ a.u. The H_2 polarization radius was estimated by scaling the H value with polarizability: $R_{\rm H_2}\approx R_{\rm H}(\alpha_{\rm H_2}/\alpha_{\rm H})^{1/3}\approx 1.55$ a.u. These radii are ≈50% smaller than the ones used in the original calculations, increasing $F_{\rm pol}$ by about one order of magnitude. The $P(\rho)$ curves computed along six isotherms still display an unstable regime ($\partial P/\partial\rho<0$) and the resulting phase line is shown on Fig. 5 (dotted line). The transition pressure is lowered by ≈40%. The new critical point lies near $\log_{10}T_c=4.0$ and $P_c=0.76$ Mbar.

In Sec. III A 1, we have rejected the process of Stark ionization by the plasma microfield because the Holtsmark distribution leads to unrealistic results for $\Gamma>1$. The use of microfield distributions in the strong Coulomb coupling regime in our free-energy model is not computationally realistic at present. However this approach is well behaved up to the PPT. We have therefore estimated *ex post facto* the effect of this form of coupling upon the pressure (P) and the entropy (S) of the four-component mixture at the limit of stability of phase I. To keep this calculation simple, we have *not* computed new chemical equilibria along the PPT. This approximation is justified by the very low plasma concentration found in phase I (see Table II), which decreases the importance of the coupling terms. At a given temperature, the values of the density and of the concentrations of each species at the boundary of phase I are determined with the model described in Sec. III A 2 [Eq. (11)]. The resulting thermodynamics constitutes the "reference" calculation. We then modify the model by including Stark ionization as a coupling between charged and neutral particles, modifying the occupation probability (see Sec. III A 1), and we recompute the thermodynamics at the *same* temperature, density, and chemical equilibrium as for the reference calculation. The differences found in P and S relative to the "reference" values are listed in Table IV. We find that the pressure is more affected than the entropy but that the effect is negligible for $\log_{10}T\leq 4.10$. The importance rises rapidly near the critical point, however, following the increase in degree of ionization. Table IV indicates that Stark ionization may play an important role in determining the exact location of the critical point. Since ω_α is overestimated when using the Holtsmark microfield distribution in regimes of strong coupling ($\Gamma>1$ at the critical point), we believe that the values in Table IV for Stark ionization may be grossly overestimated.

TABLE IV. Effects of Stark ionization coupling between charged and neutral particles on the total pressure (P) and entropy (S) of the four-component mixing along the limit of stability of phase I.

$\log_{10}T$ (K)	Stark ionization	
	$\Delta P/P$	$\Delta S/S$
3.70	7.3×10^{-4}	-8.0×10^{-4}
3.86	2.4×10^{-3}	-1.5×10^{-3}
4.02	0.011	-3.6×10^{-3}
4.185	0.38	−0.056

2. H_2 internal partition function

We have not included the experimentally observed softening of the vibron frequency in the internal partition function of the H_2 molecules [12]. For $\log_{10}T \geq 3.86$, the shift in frequency is less than 4% at the transition pressure for the $\mathbf{k}=0$ phonon mode. At lower temperatures, the effect becomes more important, and the frequency shift reaches 10% at the lowest temperature given in Table II. We have recomputed the transition pressure with the model given by Eq. (11) for the $\log_{10}T=3.86$ isotherm, after reducing the constant W_e in the internal partition function of H_2 [Eqs. (20) and (21) of Paper I] by 4%. This raises the transition pressure by 1%, as shown by the open circle in Fig. 5. Note that if we consider all phonons in the Brillouin zone, we expect little softening of the vibron mode and the effect will therefore be entirely negligible.

Another important issue in our calculations is the rotation partition function of H_2. The asymmetry of the H_2-H_2 potential is expected to hinder rotation at high pressure, which can be interpreted as an increase of the rotation temperature $\Theta_{\rm rot}$ (see Sec. III A 1 of Paper I). That could decrease substantially the entropy of the molecular phase and affect the location and the existence of the PPT. Our treatment uses the rotation temperature of the free molecule (≈ 85 K) at all densities. Recent experiments [52] show that H_2 molecules undergo significant rotational motion up to 1.6 Mbar at 77 K, a pressure typical of the PPT coexistence curve. Interestingly, the Raman spectrum of the roton modes does not show any line shifts of consequence for the EOS: $\Theta_{\rm rot}$ appears to be nearly independent of pressure, well above the PPT. Moreover, in the *fluid* state, at $T \gtrsim 10^3$ K, where there is no symmetry in the spatial distribution of molecules and where thermal effects are important, we suspect that rotational modes freeze at much higher pressures than is observed experimentally below room temperature. Therefore, we feel that our treatment is justified in the lack of better information.

3. Repulsive cores

The only *ad hoc* feature of our free-energy model consists of the arbitrary stiffening of the interatomic potentials by introducing infinitely repulsive cores [Eq. (14)] in order to obtain complete pressure ionization at the highest densities. We have therefore computed the transition pressure for the $\log_{10}T=3.86$ and 4.10 isotherms, using the same model as the "original" PPT (solid curve) but with no hard cores in the interatomic potentials [$\sigma_{ij}^0=0$ in Eq. (14)]. In this case, we find that the transition pressure is barely affected, as shown by the squares on Fig. 5. Because the equation of state is softer, the values of the density of each phase at the transition are increased by about 8%. As a final variation, we indicate the forced phase transition by the dashed line in Fig. 5. The results of these various calculations are summarized in Table V.

4. Softening of the potentials

Recently Hemley *et al.* [53] derived a new experimentally determined H_2-H_2 potential based on X-ray-diffraction measurements of solid H_2 at $T=300$ K and $P \lesssim 0.26$ Mbar [54]. This potential is slightly softer than the potential we have used [55,16]. Given the lack of information for the H-H and H-H_2 potentials at high density, we mimicked many-body effects by softening arbitrarily the repulsive part of the potentials by $\approx 20\%$ for H-H and $\approx 35\%$ for H-H_2, as discussed in Paper I.

We recomputed the chemical equilibrium with these three pair potentials for four isotherms. Results are shown by asterisks in Fig. 5. In all cases, $P_{\rm trans}$, $\rho^{\rm I}$, and $\rho^{\rm II}$ increase slightly, as expected for a softened EOS in phase I. The degree of ionization in phase II is raised by $\approx 5\%$. Ionization occurs in the same abrupt fashion as with the original potentials, and full ionization is reached in the same density range. In summary, the softened potentials do not change any of the qualitative features of the PPT and the magnitude of the effect is less than 5%.

5. Strong ion-electron coupling

Finally we tried to evaluate the consequence of strong coupling effects between ions and electrons in the fully ionized plasma on the PPT. We performed additional calculations using the fit of Tanaka, Yan, and Ichimaru [35] (hereafter, TYI) for the free energy of the plasma phase. That led to completely nonrealistic results, including full pressure ionization at very low densities,

TABLE V. Summary of the various plasma phase transition calculations displayed in Fig. 5.

Symbol	Hard cores	Coupling	$\log_{10}T_c$	Comments
– – –	yes	No mixing		Forced transition
——	yes	$F_{\rm pol}$	4.185	PPT, Eq. (11)
×	yes	$5F_{\rm pol}$	4.175	Ref. [44]
□	no	$F_{\rm pol}$	?	
△	no	none	4.215	
○	yes	$F_{\rm pol}$	?	4% vibron softening
*	yes	$F_{\rm pol}$	?	Softened potentials
- - - - -	yes	$F_{\rm pol}$	≈ 4.0	Pol. radius of Ref. [51]

where the validity of our free-energy model for H-H_2 mixtures has been demonstrated by comparison with experimental results. A *forced* phase transition computed between our neutral H-H_2 model and the TYI EOS gives a pressure transition $P \approx 0.008-0.06$ Mbar for $\log_{10} T \approx 3.9-4.1$, at densities so low that the fluid is barely nonideal. That clearly shows that the TYI theory is not compatible with a theory that includes bound states explicitly, most probably because strong nonlinear effects in the TYI theory mimic in fact the presence of bound states. Moreover, the ion-electron pair-correlation function and the plasma total interaction energy per particle in the TYI model recovers the isolated atom limit (*in its ground state*) for $\Gamma \approx 1$ and $\Theta = 1$, where thermal excitation of H atoms as well as interactions with the surrounding plasma (see Fig. 8) are significant. Therefore we do not understand why their model reaches a limit characteristic of the isolated atom.

In any event, an exact theory for describing strong ion-electron correlations in a plasma has not been issued yet, and the existing theories break down when a significant number of bound states is involved [56]. We expect the ion-electron's nonlinear effects in the plasma phase to lower slightly its free energy (by a few percent around the critical point, see Sec. II), favoring ionization. The same effect is expected from a proper inclusion of microfield effects in the ionized phase. Therefore the critical temperature shown in Fig. 3 may be overestimated.

In conclusion, within the general framework of our free-energy model, the PPT appears to stand on firm ground. Not only do we find a phase transition in all cases studied here (it is conceivable that the modified models described above could have predicted *gradual* pressure ionization), but also the five conclusions of Sec. V A remain valid. In addition to these qualitative aspects, Fig. 5 indicates that the location of the coexistence curve and of the critical point in particular are fairly insensitive to a number of important features of the free-energy model. The main *quantitative* effect arises from a modification of the hard cores entering the polarization potential of Eq. (5).

A potentially important aspect of pressure ionization we have ignored is the onset of delocalization of the electronic wave functions at high density, leading to possible electronic "conduction bands" in the neutral mixture. This phenomena is similar to the narrowing of band gaps in solids. Friedli and Ashcroft [5] have performed zero-temperature band-structure calculations for the hydrogen molecule (assuming fixed molecular bond length). However, the computation of electron delocalization in a finite-temperature fluid is a very difficult task. We estimated the size of the effect in an *ex post facto* calculation. We used the zero-temperature band-gap calculation of Friedli and Ashcroft as fitted by Ross and Lee [57]. The fraction of electrons thermally excited into the conduction band varies from less than 10% at 8000 K to 2% at the critical point. Consequently we find the effect on the PPT to be small. Moreover, as discussed previously, the H_2 molecule is likely to undergo substantial rotation at pressures characteristic of the PPT, which probably widens the band gap.

C. High-pressure experiments and the plasma phase transition

The behavior of solid hydrogen under high pressure is a rapidly unfolding experimental field, thanks to considerable progress in the technique of static compression with diamond anvil cells over the past few years. It appears that early claims of observation of a metallic phase of hydrogen are not readily supported by more recent evidence. While the observed behavior is usually found to be *consistent* with a metallic state, no incontrovertible evidence for metallization has been presented.

Hemley and Mao [14] have reported measurements of the frequency of intramolecular vibration of H_2 in the fundamental mode (the "vibron frequency") under pressures up to and above 2 Mbar and temperatures up to 300 K. These authors found a discontinuity in the vibron frequency for pressures above ~ 1.5 Mbar, which is associated with a phase transition with a critical point at $T_c \approx 150$ K and $P_c \approx 1.5-1.7$ Mbar [14]. This transition appears to be *electronic* in nature, rather than structural, and could be due to the closure of the indirect band gap [52,58], characterizing a *semimetal* state. These experiments have *not* probed the metallic regime so far and it is possible that the vibron discontinuity is associated with a low-temperature excitonic phase or, alternatively, with an orientational transition [59]. Closure of the *direct* gap, and hence metallization, is believed to occur at $P \gtrsim 3$ Mbar [59–61]. This does not put a strong constraint on our estimate of the PPT, since these are essentially zero-temperature experiments, but we note that our coexistence curve is consistent with the observed high-pressure behavior of hydrogen.

The general concept of a first-order PPT has received some experimental support from liquid-state and solid-state physics. Dielectric anomalies and an abrupt variation of the electrical conductivity, figuring a metal-insulator transition, have been observed along the liquid-vapor curve in Cs and Rb [62]. The electron-hole liquid observed in cooled silicon and germanium [63,64] *does* exhibit such a metal-insulator phase transition. As density increases, the excitons photogenerated in the semiconductor pass through a gas-liquid transition, forming the so-called electron-hole liquid in which electrons and holes become unbound (excitons are "ionized," in our language). This suggests that a metal-insulator transition is also taking place. Smith and Wolfe [65] have in fact observed this transition directly in silicon and have found a second critical point at $T_c = 45 \pm 5$ K and density of $n_c = 2.3 \times 10^{17}$ cm^{-3}. Exploiting the similarities between excitons and hydrogen atoms [40], one can use simple scaling relations for the second critical point to relate the measurements for the electron-hole liquid to theoretical predictions for pressure ionization of hydrogen. Assuming that kT_c scales as the ionization energy of the system (H atom or exciton) and that the critical density n_c is given by equating the Fermi energy of the free electrons to the ionization energy, one obtains

$$kT_c \propto \epsilon_*^{-2} m_* , \quad n_c \propto \epsilon_*^{-3} m_*^3 , \tag{18}$$

where ϵ_* is the dielectric constant of the medium and m_*

TABLE VI. Equation of state along the $\log_{10}T=3.86$ isotherm. For each density ρ, we give the number concentrations of atoms, molecules, and protons as well as the pressure, the internal energy, and the entropy. Recall that $0\leq x_{H^+}\leq 0.5$.

$\log_{10}\rho$ (g/cm^3)	x_H	x_{H_2}	x_{H^+}	$\log_{10}P$ (erg/cm^3)	$\log_{10}U$ (erg/g)	$\log_{10}S$ (erg/g K)
−6.0	9.9766×10^{-1}	4.8178×10^{-4}	9.3053×10^{-4}	5.7766	12.4844	9.2782
−5.0	9.9464×10^{-1}	4.7654×10^{-3}	2.9560×10^{-4}	6.7745	12.4807	9.2315
−4.0	9.5726×10^{-1}	4.2555×10^{-2}	9.4418×10^{-5}	7.7585	12.4590	9.1753
−3.0	7.6760×10^{-1}	2.3234×10^{-1}	3.0221×10^{-5}	8.6872	12.3589	9.0952
−2.0	4.2695×10^{-1}	5.7303×10^{-1}	9.5974×10^{-6}	9.5954	12.1999	9.0043
−1.0	1.7095×10^{-1}	8.2904×10^{-1}	6.5601×10^{-6}	10.6830	12.1059	8.9235
−0.5	1.1115×10^{-1}	8.8870×10^{-1}	7.8931×10^{-5}	11.5183	12.1542	8.8760
0.0	7.4500×10^{-2}	3.4297×10^{-1}	2.9126×10^{-1}	12.4101	12.5237	8.8462
0.5	0	0	0.5	13.4987	12.9457	8.7067
1.0	0	0	0.5	14.4616	13.4581	8.5786

is the effective mass of the electron. Scaling down our second critical point for hydrogen ($T_c=15\,300$ K, $n_c=1.86\times10^{22}$ cm^{-3}) to the electron-hole liquid in silicon, we get $T_c=27.4$ K and $n_c=1.8\times10^{17}$ cm^{-3}, close to the experimental values, adding titillating support to the existence of a plasma phase transition in hydrogen.

VI. RELATIVE IMPORTANCE OF THE DIFFERENT CONTRIBUTIONS TO THE FREE ENERGY

A small subset of our EOS results is presented in Tables VI–VIII and Figs. 6–8, each corresponding to an isotherm. For each density point in the tables, we give the abundances of H, H_2, and H^+ at chemical equilibrium, along with the total pressure, internal energy, and entropy.

Figures 6–8 show the relative importance of the different contributions to the free energy along representative isotherms. The vertical scale is the logarithm of the absolute value of the dimensionless free energy *per proton* (bound or unbound). To keep the figures relatively simple, we have grouped the various contributions (all dimensionless) to the total free energy as follows. F is the total free energy (thick solid line); F_1 (short-dashed line) is the ideal contribution *from all species present*, including electron degeneracy; F_2 (dot–short-dashed line) is the internal free energy of hydrogen molecules *and* atoms, treated within the occupation probability formalism; F_3 (long-dashed line) is the configuration free energy of the $H+H_2$ mixture (hard-sphere free energy and perturbation), *without* the linear, excluded-volume part of the hard-sphere free energy (see Sec. IV A of Paper I), which is implicitly included in F_2; F_4 (dot–long-dashed line) is the $\hbar^2$ quantum correction for atoms and molecules [Eq. (23) of Paper I]; F_5 (short-dashed–long-dashed line) includes all nonideal terms of the plasma free energy (2) [note that this term also includes the contribution given in Eq. (3) so that it eventually becomes positive]. Finally, F_6 (thin solid line) is the polarization free energy [Eq. (9)]. The behavior of these curves reflects not only the density dependence of the corresponding term but also the varying chemical equilibrium along the isotherm.

Figure 6 shows the $\log_{10}T=3.86$ isotherm, which crosses very different physical regimes. At low density ($\log_{10}\rho\lesssim-4$), the fluid is almost entirely composed of atoms and as the density rises, the chemical equilibrium shifts toward a molecular state. This behavior, together with the density dependence of F_2, F_3, and F_4, is com-

TABLE VII. Same as Table VI for $\log_{10}T=4.18$.

$\log_{10}\rho$ (g/cm^3)	x_H	x_{H_2}	x_{H^+}	$\log_{10}P$ (erg/cm^3)	$\log_{10}U$ (erg/g)	$\log_{10}S$ (erg/g K)
−6.0	4.5181×10^{-1}	4.0391×10^{-6}	2.7409×10^{-1}	6.2363	12.9932	9.3881
−5.0	7.4860×10^{-1}	9.4652×10^{-5}	1.2565×10^{-1}	7.1544	12.7956	9.2943
−4.0	9.0387×10^{-1}	1.2760×10^{-3}	4.7428×10^{-2}	8.1165	12.6805	9.2219
−3.0	9.5227×10^{-1}	1.3641×10^{-2}	1.7045×10^{-2}	9.0985	12.6270	9.1570
−2.0	8.7353×10^{-1}	1.0730×10^{-1}	9.5856×10^{-3}	10.0656	12.5743	9.0859
−1.0	5.6894×10^{-1}	4.1542×10^{-1}	7.8193×10^{-3}	11.0588	12.4683	8.9979
−0.5	3.6790×10^{-1}	5.8654×10^{-1}	2.2780×10^{-2}	11.7530	12.4566	8.9479
0.0	1.1551×10^{-1}	1.9116×10^{-1}	3.4667×10^{-1}	12.4900	12.6649	8.9169
0.5	0	0	0.5	13.5374	13.0091	8.8053
1.0	0	0	0.5	14.4747	13.4786	8.7056
1.5	0	0	0.5	15.3729	13.9280	8.5801

TABLE VIII. Same as Table VI for $\log_{10}T=4.50$

$\log_{10}\rho$ (g/cm^3)	x_H	x_{H_2}	x_{H^+}	$\log_{10}P$ (erg/cm^3)	$\log_{10}U$ (erg/g)	$\log_{10}S$ (erg/g K)
−6.0	3.6218×10^{-2}	9.0288×10^{-11}	4.8189×10^{-1}	6.7079	13.3548	9.4929
−5.0	8.4550×10^{-2}	2.6043×10^{-8}	4.5773×10^{-1}	7.6919	13.3396	9.4346
−4.0	1.9754×10^{-1}	7.2618×10^{-6}	4.0123×10^{-1}	8.6374	13.2785	9.3607
−3.0	4.0466×10^{-1}	5.4169×10^{-4}	2.9740×10^{-1}	9.5490	13.1443	9.2670
−2.0	5.6095×10^{-1}	1.0472×10^{-2}	2.1429×10^{-1}	10.4837	13.0038	9.1731
−1.0	4.3791×10^{-1}	6.0387×10^{-2}	2.5085×10^{-1}	11.4274	12.9000	9.0849
0.0	1.4876×10^{-1}	8.4305×10^{-2}	3.8347×10^{-1}	12.6841	12.8577	8.9736
1.0	0	0	0.5	14.5006	13.5185	8.8044
2.0	0	0	0.5	16.2523	14.3481	8.5938

mented on in Paper I. Up to $\log_{10}\rho\approx-1$, the main contribution to the free energy arises from the kinetic terms and eventually from the internal structure contribution of atoms and molecules. Above this density, the configuration term F_3 in the H-H_2 mixture becomes significant, and ultimately dominant. The contributions of the H-H_2 mixture largely dominate ionic contributions, given the very low degree of ionization (see Table VI).

Near $\log_{10}\rho\approx-0.15$, all curves show a common gap that corresponds to the PPT. Above the PPT, full ionization is reached rapidly, as shown by the dramatic drop in the neutral particle contributions F_2, F_3, F_4, and also the coupling term F_6. Above $\log_{10}\rho=0.5$, we are in the strongly coupled ($\Gamma>10$), strongly degenerate ($\Theta<0.1$) plasma, where the nonideal terms ($F_5<0$) are comparable to the kinetic contribution (F_1). Note that the sudden jump in ionization fraction across the PPT (see Fig. 4) is reflected in the large discontinuity in F_5. The quantum correction is everywhere negligible, except in the high-density limit of phase I.

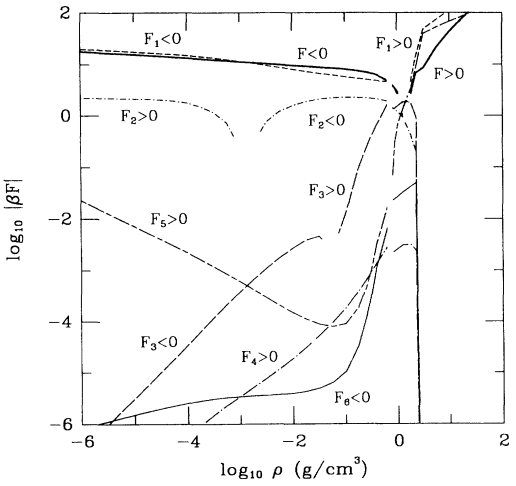

FIG. 6. Individual contributions to the free energy along the $\log_{10}T=3.86$ isotherm. The quantity plotted is $\log_{10}|\beta F|$, where F is the free energy *per proton*. The value of $\log_{10}|\beta F|$ diverges negatively where the free energy changes sign, indicated by a gap in some curves, as for F_3 near $\log_{10}\rho=-1.2$. The total free energy is shown by the thick solid line. Contributions to the free energy are labeled as follows. F_1, kinetic; F_2, bound states; F_3, neutral interactions; F_4, neutral quantum correction; F_5, all nonideal plasma terms; F_6, polarization. The gap in all curves at $\log_{10}\rho=-0.15$ corresponds to the PPT.

The second isotherm shown is just below the critical temperature at $\log_{10}T=4.18$ (Fig.7). Again, the fluid is nearly ideal below the PPT, the main nonkinetic contribution still coming from the internal free energy F_2. Note that the density dependence of F_2, reflecting the recombination of atoms into molecules, is now more important. As the temperature increases for a given density, the fluid becomes more ideal and the occupation probabilities ω_α, and therefore the degree of excitation, also increase [see Eq. (16) and Fig. 6 of Paper I].

The behavior of F_2 above $\log_{10}\rho\approx-2$ deserves more comments. As the density rises, F_2 first decreases (remember that $F_2<0$ for molecules), a direct consequence of molecular recombination (see Sec. VIII D of Paper I) and of the removal of states from the internal partition function (IPF). Then, above the PPT, ionization proceeds rapidly, causing F_2 to decrease abruptly. The plasma correlation energy, the dominant nonideal contribution at very low density, first decreases with increasing density due to recombination, but it overcomes all the other contributions above the PPT except for the kinetic terms (note that $F_5<0$ for $\log_{10}\rho>-0.3$). Of

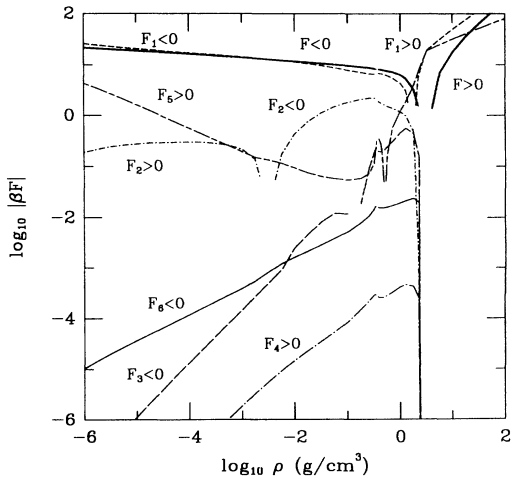

FIG. 7. Same as Fig. 6, for $\log_{10}T=4.18$. The narrow gap in all curves at $\log_{10}\rho=-0.45$ corresponds to the PPT.

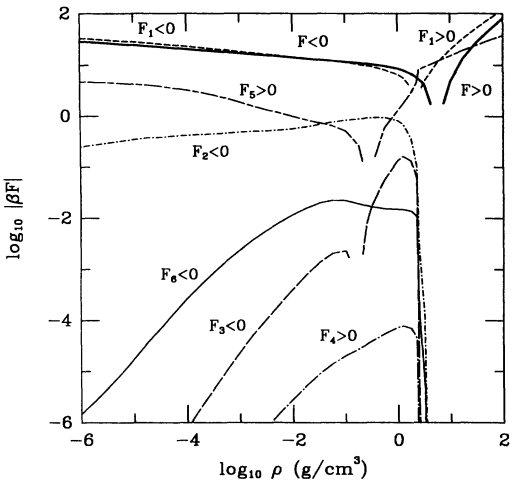

FIG. 8. Same as Fig. 6, for $\log_{10}T=4.50$.

course, F_5 and the polarization contribution F_6 increase with temperature, reflecting temperature ionization.

Figure 8 shows the $\log_{10}T=4.50$ isotherm, a temperature above the critical temperature of the PPT. Temperature ionization becomes important (Table VIII) and the plasma energy is the main nonideal contribution over the whole density range. The plasma coupling is small at low density ($\Gamma \lesssim 1$), and F coincides with the ideal term F_1. As soon as pressure ionization occurs ($\log_{10}\rho \gtrsim 0$), $\Gamma \gtrsim 3$ and the nonideal terms dominant in the plasma until electron degeneracy takes precedence. Note that $|F_5|$ increases with density. Finally, the contributions F_2, F_3, and F_6 initially increase in magnitude as the concentration of atoms increases but quickly vanish above $\log_{10}\rho \approx 0$ because of pressure ionization.

In summary, hydrogen is nearly ideal at densities below $\log_{10}\rho \approx -2$, where approximate theories for the interactions can be used successfully for most practical applications. Nonideal contributions arise principally from the internal level contributions of H and H_2 at low temperature, and from the plasma contribution as temperature ionization proceeds. At higher densities, however, interactions become so strong that detailed theories and models are required if we aim at a realistic description of pressure ionization.

TABLE IX. Details of the internal partition function of H and H_2 along the $\log_{10}T=3.86$ isotherm. The occupation probability of the ground state is ω_1. A measure of the degree of excitation is given by N_2/N_1, the ratio of the population of the first excited state to that of the ground state. For the molecule, level 2 is the first excited vibrational state.

$\log_{10}\rho$ (g/cm^3)	H_2		H	
	ω_1	N_2/N_1	ω_1	N_2/N_1
−4.0	0.999	0.470	1.000	3.20×10^{-7}
−3.0	0.995	0.470	0.996	3.09×10^{-7}
−2.0	0.953	0.469	0.967	2.37×10^{-7}
−1.5	0.865	0.467	0.902	1.32×10^{-7}
−1.0	0.646	0.461	0.734	2.31×10^{-8}
−0.5	0.370	0.451	0.475	4.88×10^{-10}
0.0	0.210	0.440	0.307	8.86×10^{-12}

TABLE X. Same as Table IX for $\log_{10}T=4.18$.

$\log_{10}\rho$ (g/cm^3)	H_2		H	
	ω_1	N_2/N_1	ω_1	N_2/N_1
−4.0	1.000	0.702	1.000	1.60×10^{-3}
−3.0	0.996	0.702	0.997	1.56×10^{-3}
−2.0	0.959	0.700	0.972	1.21×10^{-3}
−1.5	0.882	0.698	0.919	7.10×10^{-4}
−1.0	0.697	0.691	0.781	1.65×10^{-4}
−0.5	0.435	0.677	0.550	7.45×10^{-6}
0.0	0.275	0.664	0.396	3.98×10^{-7}

Tables IX–XI display the relative contributions of the first excited states of H and H_2 to the IPF along the same three isotherms. For the two lowest temperatures, the atom is found to remain in its ground state, while the first excited vibrational state of H_2 contributes appreciably to the IPF. As the temperature increases, N_2/N_1 increases due to thermal excitation and also because the occupation probability ω_α increases as the fluid becomes more ideal. For the highest isotherm, about 10% of the H atoms are in the first excited state at lowest density. Then the contribution decreases as the atomic packing fraction increases. The sudden increase in N_2/N_1 at $\log_{10}\rho=0.5$ is clearly not physical and stems from the absence of Stark ionization in our theory, leading to an underestimation of the degree of ionization when it approaches unity.

VII. CONCLUSION

Despite the shortcomings of the chemical picture, our model represents a reasonable description of pressure ionization of hydrogen in the high-temperature fluid with a single model based on first principles. We have made significant progress in the study of the plasma phase transition. Limited exploration of the sensitivity of the PPT to various model parameters and forms of neutral-charged coupling indicate that its existence is rather well established *within the general framework of our model.* However, we cannot exclude the possibility that the PPT may be an inherent feature of the model or a consequence of applying the chemical picture in a regime where it fails to account adequately for the actual physical behavior of matter. For instance, it is still conceivable that pressure

TABLE XI. Same as Table IX for $\log_{10}T=4.50$.

$\log_{10}\rho$ (g/cm^3)	H_2		H	
	ω_1	N_2/N_1	ω_1	N_2/N_1
−4.0	1.000	0.832	1.000	9.47×10^{-2}
−3.0	0.998	0.832	0.999	9.35×10^{-2}
−2.0	0.975	0.831	0.984	8.00×10^{-2}
−1.5	0.922	0.829	0.949	5.55×10^{-2}
−1.0	0.799	0.824	0.863	2.19×10^{-2}
−0.5	0.597	0.813	0.706	3.30×10^{-3}
0.0	0.355	0.795	0.493	1.28×10^{-4}
0.5			0.999	9.38×10^{-2}

ionization may occur smoothly by closure of a "conduction gap." Experimental studies will be necessary to resolve these issues and to verify the existence of the PPT.

Within the framework of our model, the following picture emerges for pressure dissociation and ionization of fluid hydrogen. Below pressure ionization, the system is essentially neutral and mostly in a molecular state; the maximum of molecular concentration is reached for $\log_{10}\rho \approx -0.5$. Dissociation occurs mainly because of temperature effects. Partial ionization occurs as the PPT is crossed, most of the ionization occurring at the expense of the molecules. The concentration of atoms remains small ($x_H \leq 10\%$), so that only two main states coexist (H_2 and H^+), in agreement with pressure ionization as described by the *physical* picture [66]. As the density is further increased, molecules disappear and ionization proceeds smoothly over a relatively narrow density range.

A question still remains: what causes the PPT, if it exists? As discussed in Sec. V, the nature of the PPT appears to be based on the nature of the potential of mean force felt by the particles in the neutral and plasma phases. As the density increases, this potential will change from a strongly repulsive interatomic potential into a softer Yukawa-type potential, increasing appreciably the phase space available to the particles. Figure 9 shows a comparison between effective interatomic and interionic potentials near the critical density for two isotherms below and above the critical temperature. The figure clearly shows the large differences between the H_2-H_2 potential, characteristic of the neutral phase (recall that $x_H < 10\%$ along the PPT), and the effective screened interionic potential given by Eq. (1). The linear screening theory overestimates the extent of screening, and as a result, the interionic potential is too repulsive [67,19], as seen in Fig. 9(b). The actual difference between the two types of potentials is certainly more pronounced than suggested by Fig. 9(a). Given the large difference between these two potentials, we can expect a discontinuity in the average interaction energy, and then an abrupt change in the two-particle distribution function. At high temperature (Fig. 9(b)), the dominant neutral species is *atomic* hydrogen. The repulsive part of the H-H potential is similar to the screened interionic potential and ionization occurs smoothly. In terms of correlation lengths that characterize the many-body effects, the system will collapse from a dense molecular phase characterized by a length λ_{H_2} into a metallic phase characterized by a new *screening* length $\lambda_e \ll \lambda_{H_2}$. In this sense the PPT can be related to the metal-insulator transition in metals associated with the liquid-vapor transition [62]. In the metal, the bare ion-ion interactions are screened by the delocalized electrons and differ considerably from the interactions between the electron-bound ions in the vapor. This crucial difference between the two effective interactions in the metallic and insulating phases, which reflects a change of the nature of the electronic states, leads eventually to a polarization catastrophe and the impending insulator-metal transition [68].

Besides its intrinsic theoretical interest, the phase diagram of hydrogen is also of major interest for astrophysical applications. Indeed, hydrogen is the major constituent of stellar matter and pressure ionization occurs in various astrophysical objects. If this phenomenon occurs through a first-order phase transition, it will have important consequences on the interior structure of giant planets and the evolution of low-mass stars [2,69,70]. Therefore the experimental quest for pressure ionization of hydrogen and an understanding of the very nature of its insulator-metal transition remain one of the most important problems of dense-matter physics.

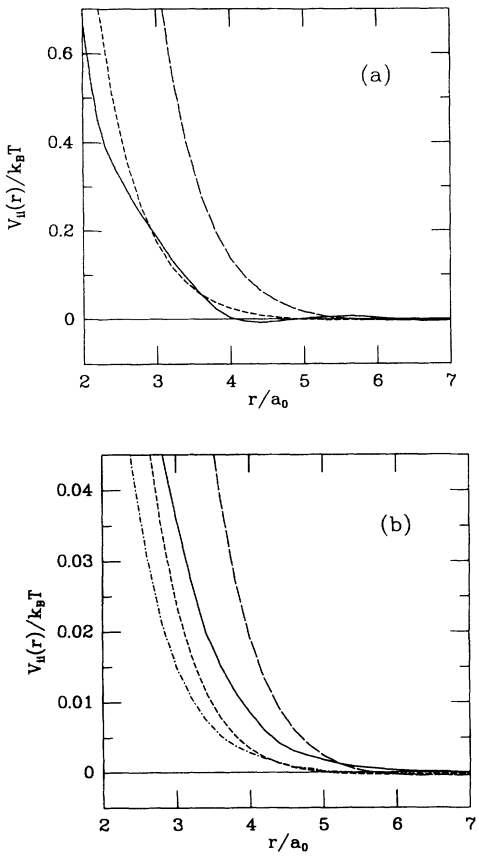

FIG. 9. Comparison of effective pair potentials. Solid line, effective interionic potential calculated with the SOCP model [Eq. (1)]; long-dash line, H_2-H_2 potential [55]; short-dashed line, H-H potential [16]. (a) $\log_{10}T=4$ and $\rho=0.6$ g/cm^3. (b) $\log_{10}T=4.86$ and $\rho=0.33$ g/cm^3. The dash-dot curve shows the effective interionic potential calculated within the framework of the density functional theory [36].

ACKNOWLEDGMENTS

We wish to thank H. M. Van Horn for his continuous interest in this work, and F. H. Ree, M. Ross, F. J. Rogers, and W. Kraeft for helpful discussions. D.S. gratefully acknowledges financial support from the Natural Sciences and Engineering Research Council of Canada. We are grateful to the Vice Provost for Computing of

the University of Rochester for making available to us the substantial computer resources required to complete this project. This work was supported in part by NSF Grant Nos. AST-87-06711, AST-91-15132, and PHY-88-08146 and by NASA Grant Nos. NAGW-1476, NAGW-2262, and NAGW-2444 through the University of Rochester. The Laboratoire de Physique, Ecole Normale Supérieure de Lyon, is an "Equipe associée au CNRS."

[1] E. Wigner and H. B. Huntington, J. Chem. Phys. **3**, 764 (1935).
[2] D. J. Stevensen and E. E. Salpeter, Astrophys. J. Suppl. Ser. **35**, 221 (1977).
[3] W. Ebeling and W. Richert, Phys. Lett. **108A**, 80 (1985).
[4] W. Ebeling and W. Richert, Phys. Status Solidi **128**, 467 (1985).
[5] C. Friedli and N. W. Ashcroft, Phys. Rev. A **16**, 662 (1977).
[6] S. Chakravarty, J. H. Rose, D. Wood, and N. W. Ashcroft, Phys. Rev. A **24**, 1624 (1985).
[7] D. Ceperley and B. J. Alder, Phys. Rev. A **36**, 2092 (1987).
[8] B. I. Min, H. J. F. Jansen, and A. J. Freeman, Phys. Rev. A **33**, 6383 (1986).
[9] T. W. Barbee III, A. García, M. L. Cohen, and J. L. Martins, Phys. Rev. Lett. **62**, 1150 (1989).
[10] M. van Thiel, L. B. Hord, W. H. Gust, A. C. Mitchell, M. D'Addario, K. Boutwell, E. Wilbarger, and B. Barret, Phys. Earth Planet. Inter. **9**, 57 (1974).
[11] W. J. Nellis, A. C. Mitchell, M. van Thiel, G. J. Devine, and R. J. Trainor, J. Chem. Phys. **79**, 1480 (1983).
[12] R. J. Hemley and H. K. Mao, Phys. Rev. Lett. **61**, 857 (1988).
[13] H. E. Lorenzana, I. F. Silvera, and K. A. Goettel, Phys. Rev. Lett. **63**, 2080 (1989).
[14] R. J. Hemley and H. K. Mao, Science **249**, 391 (1990).
[15] H. E. Lorenzana, I. F. Silvera, and K. A. Goettel, Phys. Rev. Lett. **65**, 1901 (1990).
[16] D. Saumon and G. Chabrier, Phys. Rev. A **44**, 5122 (1991) (Paper I).
[17] D. G. Hummer and D. Mihalas, Astrophys. J. **331**, 794 (1988).
[18] D. Saumon, G. Chabrier, and J. J. Weis, J. Chem. Phys. **90**, 7395 (1989).
[19] G. Chabrier, J. Phys. (Paris) **51**, 1607 (1990).
[20] N. W. Ashcroft and D. Stroud, in *Solid State Physics,* edited by H. Ehrenreich, F. Seitz, and D. Turnbull (Academic, New York, 1978), Vol. 33, p. 2.
[21] G. Chabrier, Phys. Lett. A **134**, 375 (1989).
[22] S. Ichimaru, H. Iyetomi, and S. Tanaka, Phys. Rep. **149**, 93 (1987).
[23] K. S. Singwi, M. P. Tosi, R. H. Land, and A. Sjölander, Phys. Rev. **176**, 589 (1970).
[24] W. L. Slattery, G. D. Doolen, and H. E. DeWitt, Phys. Rev. A **26**, 2255 (1982).
[25] D. Ceperley and B. J. Alder, Phys. Rev. A **45**, 566 (1980).
[26] S. H. Vosko, L. Wilk, and M. Nusair, Can. J. Phys. **58**, 1200 (1980).
[27] J. Lindhard, K. Dan. Vidensk. Selsk. Mat. Fys. Medd. **28**, 8 (1954).
[28] K. Utsumi and S. Ichimaru, Phys. Rev. A **26**, 603 (1982).
[29] W. B. Hubbard and W. Slattery, Astrophys. J. **168**, 131 (1971); W. B. Hubbard and H. E. DeWitt, *ibid.* **290**, 388 (1985).
[30] H. Totsuji and K. Tokami, Phys. Rev. A **30**, 3175 (1984).
[31] L. D. Landau and E. M. Lifshitz, *Course of Theoretical Physics. V. Statistical Physics,* 3rd ed. (Pergamon, Oxford, 1980), Part 1.
[32] H. Minoo, M. M. Gombert, and C. Deutsch, Phys. Rev. A **23**, 924 (1981).
[33] J. P. Hansen and I. R. McDonald, Phys. Rev. A **23**, 2041 (1981).
[34] F. Perrot, Y. Furutani, and M. W. C. Dharma-wardana, Phys. Rev. A **41**, 1096 (1990).
[35] S. Tanaka, X. Z. Yan, and S. Ichimaru, Phys. Rev. A **41**, 5616 (1990).
[36] M. W. C. Dharma-wardana, F. Perrot, and G. C. Aers, Phys. Rev. A **28**, 344 (1983).
[37] Throughout this paper, $\log_{10}T$ is the logarithm of the temperature in K, and $\log_{10}\rho$ is the logarithm of the density of g/cm^3.
[38] D. Mihalas (private communication).
[39] C. A. Iglesias, C. F. Hooper, Jr., and H. E. DeWitt, Phys. Rev. A **28**, 361 (1983).
[40] W. D. Kraeft, D. Kremp, W. Ebeling, and G. Röpke, *Quantum Statistics of Charged Particle Systems* (Plenum, New York, 1986).
[41] W. Ebeling, A. Förster, W. Richert, and H. Hess, Physica A **150**, 159 (1988).
[42] G. A. Mansoori, N. F. Carnahan, K. E. Starling, and T. W. Leland, Jr., J. Chem. Phys. **54**, 1523 (1971).
[43] W. H. Press, B. P. Flannery, S. A. Teukolsky, and W. T. Vetterling, *Numerical Recipes, The Art of Scientific Computing* (Cambridge University Press, Cambridge, 1986).
[44] D. Saumon and G. Chabrier, Phys. Rev. Lett. **62**, 2397 (1989).
[45] M. S. Marley and W. B. Hubbard, Icarus **73**, 53 (1988).
[46] M. Robnik and W. Kundt, Astron. Astrophys. **120**, 227 (1983).
[47] X. Z. Yan, S. t. Tsai, and S. Ichimaru, Phys. Rev. A **43**, 3057 (1991).
[48] D. Mihalas, W. Däppen, and D. G. Hummer, Astrophys. J. **331**, 815 (1988).
[49] K. Herzfeld, Phys. Rev. **29**, 701 (1927).
[50] M. Ross, J. Chem. Phys. **56**, 4651 (1972).
[51] R. Redmer, G. Röpke, and R. Zimmermann, J. Phys. B **20**, 4069 (1987).
[52] R. J. Hemley, H. K. Mao, and J. F. Shu, Phys. Rev. Lett. **65**, 2670 (1990).
[53] R. J. Hemley, H. K. Mao, L. W. Finger, A. P. Jephcoat, R. M. Hazen, and C. S. Zha, Phys. Rev. B **42**, 6458 (1990).
[54] The correct coefficients in Eq. (16) of Ref. [53] are $a_1 = +4.287\times10^{-4}$ hartree/bohr^3 and $a_2 = -6.718\times10^{-5}$ hartree/bohr^6 [R. J. Hemley (private communication)].
[55] M. Ross, F. H. Ree, and D. A. Young, J. Chem. Phys. **79**, 1487 (1983).
[56] J. Chihara, Phys. Rev. A **44**, 1247 (1991); **44**, 8446 (1991).
[57] M. Ross and Y. Lee (unpublished).
[58] R. J. Hemley, M. Hanfland, and H. K. Mao, Nature **350**, 488 (1991).
[59] E. Kaxiras, J. Broughton, and R. J. Hemley, Phys. Rev.

Lett. **67**, 1138 (1991).
[60] H. K. Mao and R. J. Hemley, Science **244**, 1462 (1989).
[61] J. H. Eggert, F. Moshary, W. J. Evans, H. E. Lorenzana, K. A. Goettel, I. F. Silvera, and W. C. Moss, Phys. Rev. Lett. **66**, 193 (1991).
[62] S. Jüngst, B. Knuth, and F. Hensel, Phys. Rev. Lett. **55**, 2160 (1985).
[63] T. M. Rice, in *Solid State Physics,* edited by H. Ehrenreich, F. Seitz, and D. Turnbull (Academic, New York, 1977), Vol. 32, p. 1.
[64] J. C. Hensel, T. G. Phillips, and G. A. Thomas, in *Solid State Physics* (Ref. [63]), p. 87.
[65] L. M. Smith and J. P. Wolfe, Phys. Rev. Lett. **57**, 2314 (1986).
[66] F. J. Rogers, Phys. Rev. A **29**, 868 (1984), and references therein.
[67] F. Perrot, Phys. Rev. A **25**, 489 (1982).
[68] R. E. Goldstein and N. W. Ashcroft, Phys. Rev. Lett. **55**, 2164 (1985).
[69] G. Chabrier, D. Saumon, W. B. Hubbard, and J. I. Lunine, Astrophys. J. **391**, 817 (1992).
[70] D. Saumon, W. B. Hubbard, G. Chabrier, H. M. Van Horn, Astrophys. J. **391**, 827 (1992).
[71] R. D. Dick and G. I. Kerley, J. Chem. Phys. **73**, 5264 (1980).
[72] H. K. Mao, P. M. Bell, and R. J. Hemley, Phys. Rev. Lett. **55**, 99 (1985).
[73] J. von Straaten and J. F. Silvera, Phys. Rev. B **37**, 1989 (1988).